Linear Matrix Inequalities for Physically Consistent Inertial Parameter Identification: A Statistical Perspective on the Mass Distribution

Patrick M. Wensing, Sangbae Kim, and Jean-Jacques E. Slotine

***Abstract*—With the increased application of model-based whole-body control in legged robots, there has been a resurgence of research interest into methods for accurate system identification. An important class of methods focuses on the *inertial parameters* of rigid-body systems. These parameters consist of the mass, first mass moment (related to center of mass location), and rotational inertia matrix of each link. The main contribution of this letter is to formulate physical-consistency constraints on these parameters as Linear Matrix Inequalities (LMIs). The use of these constraints in identification can accelerate convergence and increase robustness to noisy data. It is critically observed that the proposed LMIs are expressed in terms of the covariance of the mass distribution, rather than its rotational moments of inertia. With this perspective, connections to the classical problem of moments in mathematics are shown to yield new bounding-volume constraints on the mass distribution of each link. While previous work ensured physical plausibility or used convex optimization in identification, the LMIs here uniquely enable both advantages. Constraints are applied to identification of a leg for the MIT Cheetah 3 robot. Detailed properties of transmission components are identified alongside link inertias, with parameter optimization carried out to global optimality through semidefinite programming.**

***Index Terms*—Calibration and identification, dynamics.**

I. Introduction

ADVANCES in whole-body control of legged robots [1]–[4] have led to increased use of model-based methods in experimental hardware [5]–[8]. Commonly, state-of-the-art controllers perform optimization over actuator torques to generate desired motions in the robot. Recent strides in torque-controlled actuation have provided wide benefit to these techniques, and emerging actuator designs [9] suggest that performance will continue to improve. Despite these advances, the performance of whole-body control methods remains dependent on accurate dynamic models.

Manuscript received February 15, 2017; accepted July 1, 2017. Date of publication July 20, 2017; date of current version August 17, 2017. This letter was recommended for publication by Associate Editor P. Martinet and Editor K. Lynch upon evaluation of the reviewers comments. This work was supported in part by NSF through award IIS-1350879 and in part by the Agency for Defense Development of Korea under Contract UD140073ID. *(Corresponding author: Patrick M. Wensing.)*

P. M. Wensing is with the Department of Aerospace and Mechanical Engineering, University of Notre Dame, Notre Dame, IN 46556 USA (e-mail: pwensing@nd.edu).

S. Kim and J.-J. E. Slotine are with the Department of Mechanical Engineering, Massachusetts Institute of Technology, Cambridge, MA 02139 USA (e-mail: sangbae@mit.edu; jjs@mit.edu).

This paper has supplementary downloadable material available at http://ieeexplore.ieee.org.

Digital Object Identifier 10.1109/LRA.2017.2729659

Thus, recent trends in control have been accompanied by many parallel developments in the area of system identification [10]–[14]. This recent work follows a rich history of research into inertial parameter identification, with seminal work in [15]. Classically, studies have focused on challenges such as designing trajectories for optimal identification [16], [17], limiting bias from structured noise [18], [19], and verifying robustness bounds on the identified parameters [20], [21]. By comparison, recent work in the legged locomotion community has focused on challenges from the floating-base structure of legged robots [10], [11] and the use of constrained optimization to limit the search space to physically realistic parameters [12]–[14].

The floating-base structure of legged systems introduces challenges and opportunities to system identification. Pucci *et al.* [10] addressed coupling between the limbs and body to extend methods of Slotine and Li [22] for underactuated adaptive control. Other work has exploited the fact that the Newton and Euler equations of the entire robot are embedded in the dynamics of the floating base. With this property, Ayusawa *et al.* [11], [23] demonstrated that full-body inertial parameters can be estimated from contact forces and kinematics alone. These advances open the door for application to systems where joint torque measurements are not available, such as for identifying inertial parameters in humans.

Other recent work has concentrated on using constrained optimization in identification. Often, parameters are known a priori to exist within some predefined set. Such restrictions may come from considerations of physical plausibility, from bounding volumes in CAD models, or from known symmetry of a mechanism. Regardless of the source, prior knowledge can be applied to increase robustness to noisy sensors, and to accelerate model convergence [24], [25]. Convex constraints, in particular, provide desirable structure that can be naturally exploited in parameter identification and adaptive control alike. For identification, Jovic *et al.* [12] formed bounding constraints on the center of mass (CoM) of each link, and enforced symmetry of mirrored limbs. Sousa and Cortesão [13] formulated LMIs to enforce positivity of the kinetic energy. This constraint alone does not guarantee physical consistency. Recently, Traversaro *et al.* [14] described tight conditions for physical consistency of inertial parameters using a nonconvex parameterization. Optimization on manifolds was required to enforce these conditions.

A main contribution of this letter is to show how physical-consistency constraints can be expressed as LMIs on the inertial parameters. It is shown that manifold constraints from [14] can be reformulated as convex constraints through LMIs. The proposed LMIs uniquely enable globally-optimal least-squares parameter identification while enforcing plausibility of the

TABLE I
FEATURE COMPARISON

	Physical Consistency	Convex	Discrete Approx.	Uses LMIs
Sousa *et al.* [13]		✓	No	✓
Traversaro *et al.* [14]	✓		No	
Ayusawa *et al.* [23]	✓	✓	Yes	
This letter	✓	✓	No	✓

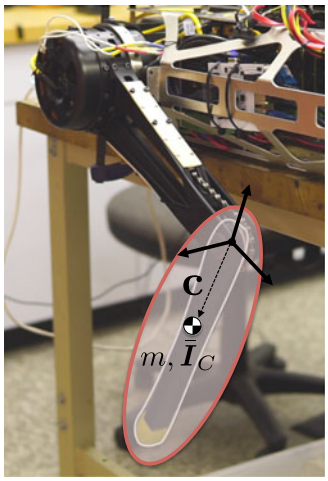

Fig. 1. Setup for system identification on the MIT Cheetah 3. This work provides new constraints to identify physically plausible masses m, center of mass locations $\mathbf{c}$, and rotational inertias $\bar{\boldsymbol{I}}_C$ through convex optimization.

result. From the form of the constraints, it is critically observed that physical consistency depends only on the covariance of the mass distribution.

This main observation stems from mathematical commonality between mass measures of rigid bodies and probability measures of random variables. This is not to say that a rigid-body has inherent stochasticity. But rather, that certifying the plausibility of moments falls to the same mathematics in both domains. This connection enables results from the classical problem of moments [26] to yield new bounding-ellipsoid constraints on the mass distribution. Formulation of these constraints is a second main contribution of the work. Although constraints are placed on the mass distribution, itself an infinite dimensional mathematical object, LMIs enable this restriction to be imposed directly on the 10 standard inertial parameters during system identification.

The letter is laid out as follows. Section II provides mathematical preliminaries. Section III reviews [13] and [14], with a high-level comparison in Table I. Section IV presents LMIs for physical consistency, highlighting connections with probability and statistics. Section V draws on these connections to introduce bounding-volume constraints. Section VI describes application to identify a leg from the MIT Cheetah 3, shown in Fig. 1. Section VII provides concluding remarks.

II. PRELIMINARIES

A. Notation and Definitions

The set of real and natural numbers are denoted by $\mathbb{R}$ and $\mathbb{N}$ respectively. $\mathbb{R}_+$ represents the set of non-negative reals. Scalars are denoted with italics $(a, b, \ldots)$, vectors with bold characters $(\mathbf{a}, \mathbf{b}, \ldots)$, and matrices with bold capitals $(\mathbf{A}, \mathbf{B}, \ldots)$. The $n \times n$ identity is noted as $\mathbf{1}_n$. The Special Orthogonal group of rotations is denoted $\mathsf{SO}(3)$, with its Lie algebra, the set of 3×3 skew-symmetric matrices $\mathsf{so}(3)$. The Special Euclidean group is denoted $\mathsf{SE}(3)$ with its Lie algebra $\mathsf{se}(3)$. The set of symmetric $n \times n$ matrices is represented as $\mathbb{S}^n$, the positive semidefinite cone $\mathbb{S}^n_+$, and the positive definite cone $\mathbb{S}^n_{++}$ [27]. The shorthand $\mathbf{A} \succeq \mathbf{B}$ indicates $\mathbf{A} - \mathbf{B} \in \mathbb{S}^n_+$ for some $n \in \mathbb{N}$. $\mathbf{A} \succ \mathbf{B}$ similarly indicates $\mathbf{A} - \mathbf{B} \in \mathbb{S}^n_{++}$.

Definition 1 (LMI Representable): A convex set $\mathcal{S} \subset \mathbb{R}^n$ is called linear matrix inequality (LMI) representable if there exists $m \in \mathbb{N}$ and constant matrices $\{\mathbf{A}_i\}_{i=0}^n \in \mathbb{S}^m$ such that

$$\mathcal{S} = \{\mathbf{x} \in \mathbb{R}^n \ : \ \mathbf{A}_0 + x_1\mathbf{A}_1 + \cdots + x_n\mathbf{A}_n \succeq \mathbf{0}\}$$

A set is called *strictly* LMI representable when the inequality can be tightened to hold strictly.

As a main benefit, a convex set $\mathcal{S}$ being LMI representable has favorable implications for optimization. Constraints of the form $\mathbf{x} \in \mathcal{S}$ can be enforced using semidefinite programming [27]. Such techniques are mature, and admit guarantees of global optimality. We refer the interested reader to [28] for further background on LMIs and their applications.

Definition 2 (Moment of a Measure): Consider a positive Borel measure μ on $\mathbb{R}^n$, $\boldsymbol{\alpha} = [\alpha_1, \ldots, \alpha_n]^\top \in \mathbb{N}^n_+$, and let $\mathbf{x}^{\boldsymbol{\alpha}} = x_1^{\alpha_1} \cdots x_n^{\alpha_n}$ for any $\mathbf{x} = [x_1, \ldots, x_n]^\top \in \mathbb{R}^n$. Then

$$\int_{\mathbb{R}^n} \mathbf{x}^{\boldsymbol{\alpha}} \, \mathrm{d}\mu(\mathbf{x})$$

is called a moment of μ, of order $|\boldsymbol{\alpha}| = \sum_{i=1}^n \alpha_i$ [26].

Any function $f : \mathbb{R}^n \to \mathbb{R}_+$ can be used to define a measure through the association $\mathrm{d}\mu(\mathbf{x}) = f(\mathbf{x})\mathrm{d}\mathbf{x}$, where $\mathrm{d}\mathbf{x}$ represents a differential volume. The general concept of a moment is applicable to both probability measures and mass measures. This commonality will be used for intuition into the LMIs that enforce plausibility of inertial parameters.

B. Rigid-Body Dynamics

The dynamics of a system of $n_b \in \mathbb{N}_+$ rigid bodies follows

$$\mathbf{H}(\mathbf{q})\,\dot{\boldsymbol{\nu}} + \mathbf{C}(\mathbf{q}, \boldsymbol{\nu})\,\boldsymbol{\nu} + \mathbf{g}(\mathbf{q}) = \boldsymbol{\tau} \tag{1}$$

where $\mathbf{H} \in \mathbb{R}^{n_d \times n_d}$ the mass matrix, $n_d \in \mathbb{N}_+$ the number of degrees of freedom, $\mathbf{q} \in \mathcal{Q}$ the configuration with $\mathcal{Q}$ the configuration manifold, $\boldsymbol{\nu} \in \mathbb{R}^{n_d}$ the generalized velocity, $\mathbf{C}\,\boldsymbol{\nu} \in \mathbb{R}^{n_d}$ and $\mathbf{g} \in \mathbb{R}^{n_d}$ the Coriolis and gravity forces, and $\boldsymbol{\tau} \in \mathbb{R}^{n_d}$ the generalized force [29]. For legged systems, the generalized force $\boldsymbol{\tau}$ has contributions from $n_j \in \mathbb{N}_+$ joint actuator torques $\boldsymbol{\tau}_j \in \mathbb{R}^{n_j}$ and $n_c \in \mathbb{N}$ external contact wrenches $\{\mathbf{f}_{c_k}\}_{k=1}^{n_c} \subset \mathbb{R}^6$ according to

$$\boldsymbol{\tau} = \mathbf{S}_j^\top \boldsymbol{\tau}_j + \sum_{k=1}^{n_c} \mathbf{J}_{c_k}^\top \mathbf{f}_{c_k}$$

where $\mathbf{S}_j \in \mathbb{R}^{n_j \times n_d}$ is an actuated joint selector matrix and $\mathbf{J}_{c_k} \in \mathbb{R}^{6 \times n_d}$ the 6D Jacobian for contact k.

It is commonly known that (1) can be represented linearly in system inertial parameters $\boldsymbol{\pi} \in \mathbb{R}^{10 n_b}$ [15]

$$\mathbf{H}(\mathbf{q})\,\dot{\boldsymbol{\nu}} + \mathbf{C}(\mathbf{q}, \boldsymbol{\nu})\,\boldsymbol{\nu} + \mathbf{g}(\mathbf{q}) = \mathbf{Y}(\mathbf{q}, \boldsymbol{\nu}, \dot{\boldsymbol{\nu}})\,\boldsymbol{\pi} \tag{2}$$

where $\mathbf{Y}$ is the regressor matrix. The parameters $\boldsymbol{\pi}$ have contributions from each body such that $\boldsymbol{\pi} = [\boldsymbol{\pi}_i^\top, \ldots, \boldsymbol{\pi}_{n_b}^\top]^\top$. The

body inertial parameters $\boldsymbol{\pi}_i \in \mathbb{R}^{10}$ are composed as

$$\boldsymbol{\pi}_i = [m, h_x, h_y, h_z, I_{xx}, I_{xy}, I_{xz}, I_{yy}, I_{yz}, I_{zz}]^\top \in \mathbb{R}^{10}$$

with m the body mass, $\mathbf{h} = [h_x, h_y, h_z]^\top = m\mathbf{c}$ the first mass moment with $\mathbf{c} \in \mathbb{R}^3$ the vector to the CoM in a body-fixed coordinate system, and

$$\bar{\boldsymbol{I}} = \begin{bmatrix} I_{xx} & I_{xy} & I_{xz} \\ I_{xy} & I_{yy} & I_{yz} \\ I_{xz} & I_{yz} & I_{zz} \end{bmatrix}$$

the rotational inertia about the coordinate origin. These parameters also describe the 6D (spatial) body inertia [29]

$$\boldsymbol{I}_i = \begin{bmatrix} \bar{\boldsymbol{I}}_i & m_i\mathbf{S}(\mathbf{c}_i) \\ m_i\mathbf{S}(\mathbf{c}_i)^\top & m_i\mathbf{1}_3 \end{bmatrix} = \begin{bmatrix} \bar{\boldsymbol{I}}_i & \mathbf{S}(\mathbf{h}_i) \\ \mathbf{S}(\mathbf{h}_i)^\top & m_i\mathbf{1}_3 \end{bmatrix} \tag{3}$$

with $\mathbf{S}(\mathbf{x}) \in \mathsf{so}(3)$ such that $\mathbf{S}(\mathbf{x})\mathbf{y} = \mathbf{x} \times \mathbf{y}, \forall\, \mathbf{x}, \mathbf{y} \in \mathbb{R}^3$.

The regressor matrix provides a simple method to pursue inertial parameter identification. Given $n_s \in \mathbb{N}_+$ samples, a least-squares identification problem can be formulated [13]

$$\min_{\boldsymbol{\pi}} \sum_{m=1}^{n_s} \|\mathbf{Y}^{(m)}\,\boldsymbol{\pi} - \boldsymbol{\tau}^{(m)}\|^2 \tag{4}$$

This optimization problem is efficiently solvable to global optimality. However, without including constraints, the optimal parameters may not correspond to any physical system.

Inertial parameters in any physical body are determined by a distribution of density $\rho_i(\cdot) : \mathbb{R}^3 \to \mathbb{R}_+$. The inertial components for each body i are a functional of $\rho_i(\cdot)$ [14]

$$m_i = \int_{\mathbb{R}^3} \rho_i(\mathbf{x})\, \mathrm{d}\mathbf{x} \tag{5}$$

$$\mathbf{h}_i = \int_{\mathbb{R}^3} \mathbf{x}\, \rho_i(\mathbf{x})\, \mathrm{d}\mathbf{x} \tag{6}$$

$$\bar{\boldsymbol{I}}_i = \int_{\mathbb{R}^3} \underbrace{\begin{bmatrix} y^2+z^2 & -xy & -xz \\ -xy & x^2+z^2 & -yz \\ -xz & -yz & x^2+y^2 \end{bmatrix}}_{\mathbf{S}(\mathbf{x})\mathbf{S}(\mathbf{x})^\top} \rho_i(\mathbf{x})\, \mathrm{d}\mathbf{x} \tag{7}$$

The moments of inertia within $\bar{\boldsymbol{I}}_i$ are not moments of $\rho(\cdot)$ in the sense of Definition 2. While $\bar{\boldsymbol{I}}_i$ is convenient to describe dynamics, the physical plausibility of inertial parameters will be more directly addressed with moments as in Definition 2.

Definition 3 (Density Realizable): Given a set $\mathcal{X} \subseteq \mathbb{R}^3$, a 6D inertia $\boldsymbol{I}$ is called $\mathcal{X}$-density realizable if $\exists \rho(\cdot) : \mathbb{R}^3 \to \mathbb{R}_+$ such that $\rho(\mathbf{x}) = 0$ when $\mathbf{x} \notin \mathcal{X}$, and the components of $\boldsymbol{I}$, $(m, \mathbf{h}, \bar{\boldsymbol{I}})$, satisfy (5)–(7). When $\mathcal{X}$ is not specified, $\mathcal{X} = \mathbb{R}^3$ is assumed.

Remark 1: Given any $\mathcal{X} \subseteq \mathbb{R}^3$, the set $\mathcal{P}^*_{\mathcal{X}}$ defined by $\mathcal{P}^*_{\mathcal{X}} = \{\boldsymbol{\pi} \in \mathbb{R}^{10} : m(\boldsymbol{\pi}) > 0,\ \boldsymbol{I}(\boldsymbol{\pi}) \text{ is } \mathcal{X}\text{−density realizable}\}$ is a convex cone. Previous work [23] provided a discrete approximation to this cone. Without discretization, the work here provides cases wherein the cone is LMI representable.

III. Previous Results

This section focuses on physical consistency for a single rigid body. As such, body indices will be dropped. Attempts to enforce physical consistency focus on the rotational inertia $\bar{\boldsymbol{I}}_C$ about the CoM. The parallel axis theorem in 3D establishes a correspondence between $\bar{\boldsymbol{I}}_C$ and $\bar{\boldsymbol{I}}$, the rotational inertia about a body-fixed coordinate origin, through

$$\bar{\boldsymbol{I}} = \bar{\boldsymbol{I}}_C + m\mathbf{S}(\mathbf{c})\mathbf{S}(\mathbf{c})^\top \tag{8}$$

A. Physical Semi-Consistency: An LMI Parameterization

Positive definite constraints on $\bar{\boldsymbol{I}}_C(\boldsymbol{\pi})$ have been commonly enforced on the inertial parameters $\boldsymbol{\pi}$ [13], [30]. In a rigid-body system, when each $m_i > 0$ and $\bar{\boldsymbol{I}}_{C_i} \succ 0$, it can be shown that $\mathbf{H}(\mathbf{q}) \succ 0\ \forall \mathbf{q} \in \mathcal{Q}$ [30]. However, these constraints are not alone enough to ensure physical consistency of the inertial parameters [14].

Definition 4 (Physical Semi-consistency): A vector of inertial parameters $\boldsymbol{\pi} \in \mathbb{R}^{10}$ is called *physically semi-consistent* if $m(\boldsymbol{\pi}) > 0$ and $\bar{\boldsymbol{I}}_C(\boldsymbol{\pi}) \succ 0$. The set of physically semi-consistent parameters is denoted $\mathcal{P} \subset \mathbb{R}^{10}$.

Theorem 1 (LMI Representation of $\mathcal{P}$): [13] The set of physically semi-consistent parameters $\mathcal{P}$ is strictly LMI representable. Its LMI representation is given as $\mathcal{P} = \{\boldsymbol{\pi} \in \mathbb{R}^{10} : \boldsymbol{I}(\boldsymbol{\pi}) \succ 0\}$.

Extending the optimization (4) to include physical semi-consistency constraints results in a semidefinite programming (SDP) problem. This problem can be solved to global optimality with SDP solvers [27]

$$\min_{\boldsymbol{\pi}} \sum_{m} \|\mathbf{Y}^{(m)}\,\boldsymbol{\pi} - \boldsymbol{\tau}^{(m)}\|^2$$
$$\text{s.t.}\ \boldsymbol{I}(\boldsymbol{\pi}_i) \succ 0 \quad \forall i \in \{1, \ldots, n_b\}$$

B. (Full) Physical Consistency: Manifold Parameterization

Definition 5 (Physical Consistency): A vector of inertial parameters $\boldsymbol{\pi} \in \mathbb{R}^{10}$ is called *physically consistent* if $m(\boldsymbol{\pi}) > 0$ and $\boldsymbol{I}(\boldsymbol{\pi})$ is density realizable. The set of physically-consistent parameters is denoted $\mathcal{P}^*$.

In comparison to $\mathcal{P}$, the set of physically consistent inertial parameters $\mathcal{P}^* \subset \mathcal{P}$ has been shown to result from only three additional conditions on $\bar{\boldsymbol{I}}_C$ [14]. These additional constraints arise from considerations regarding the principal moments of inertia. Suppose $\mathbf{R} \in \mathsf{SO}(3)$ and $\mathbf{J} = \mathrm{diag}(J_1, J_2, J_3),\ J_1, ..., J_3 > 0$ such that $\bar{\boldsymbol{I}}_C = \mathbf{R}\mathbf{J}\mathbf{R}^\top$. Then, the rotational inertia $\bar{\boldsymbol{I}}_C$ is density realizable iff

$$J_1 + J_2 \geq J_3,\ J_2 + J_3 \geq J_1, \text{ and } J_1 + J_3 \geq J_2 \tag{9}$$

Definition 6 (Triangle Inequalities): A matrix in $\mathbb{S}^3$ is said to satisfy the triangle inequalities if its eigenvalues $\{J_i\}_{i=1}^3$ satisfy (9).

Theorem 2 (Manifold Parameterization of $\mathcal{P}^*$): [14] A 6D inertia $\boldsymbol{I}$ is physically consistent if and only if there exists $m > 0, \mathbf{R} \in \mathsf{SO}(3), \mathbf{J} = \mathrm{diag}(J_1, J_2, J_3) \succ 0$ that satisfies the triangle inequalities, and $\mathbf{c} \in \mathbb{R}^3$ such that

$$\boldsymbol{I} = \begin{bmatrix} \mathbf{R}\mathbf{J}\mathbf{R}^\top + m\mathbf{S}(\mathbf{c})\mathbf{S}(\mathbf{c})^\top & m\mathbf{S}(\mathbf{c}) \\ m\mathbf{S}(\mathbf{c})^\top & m\mathbf{1}_3 \end{bmatrix}$$

Even for a single rigid body, optimization with this parameterization of $\mathcal{P}^*$ results in a nonlinear optimization problem

over a manifold

$$\min_{\mathbf{R},\mathbf{J},\mathbf{c},m} \sum_m \|\mathbf{Y}^{(m)}\,\boldsymbol{\pi}(\mathbf{R},\mathbf{J},\mathbf{c},m) - \boldsymbol{\tau}^{(m)}\|^2$$
$$\text{s.t.}\ \mathbf{R} \in \mathsf{SO}(3)$$
$$m > 0,\ J_i > 0, i = 1,2,3$$
$$J_1 + J_2 \geq J_3,\ J_2 + J_3 \geq J_1, \text{ and } J_1 + J_3 \geq J_2$$

Solution of this problem is possible using nonlinear optimization on manifolds [14]. However, this approach requires custom solvers and does not guarantee global optimality.

IV. Contribution: An LMI for Physically Consistent Inertial Parameters

This section takes a closer look at conditions for physical consistency. It is shown that the triangle inequalities can be expressed as an LMI over $\boldsymbol{\pi}$, without a manifold parametrization. First, Section IV-A describes a matrix inequality for the triangle inequalities on $\bar{\boldsymbol{I}}_C$. Intuition into this result is given in Section IV-B through introduction of the *density-weighted covariance* of a rigid body and its *covariance ellipsoid*. With this interpretation, Section IV-C develops an LMI over $\boldsymbol{\pi}$ for physical consistency. As a key benefit, this LMI enables the use of convex optimization to identify plausible parameters.

A. A Matrix Inequality for Triangle Inequalities on $\bar{\boldsymbol{I}}_C$

Suppose $\mathbf{R}$ and $\mathbf{J}$ as before such that $\bar{\boldsymbol{I}}_C = \mathbf{R}\mathbf{J}\mathbf{R}^\top$. The triangle inequalities on $\bar{\boldsymbol{I}}_C$ (9) can be rewritten as

$$J_1 + J_2 + J_3 \geq 2J_i \quad \text{i} = 1, ..., 3 \tag{10}$$

Since J_i are the eigenvalues of $\bar{\boldsymbol{I}}_C$, (10) is equivalent to

$$\tfrac{1}{2}\mathrm{Tr}(\bar{\boldsymbol{I}}_C) \geq \lambda_{\max}(\bar{\boldsymbol{I}}_C) \tag{11}$$

where $\mathrm{Tr}(\cdot)$ is the trace operator, and $\lambda_{\max}(\cdot)$ provides the maximum eigenvalue of its argument. Separately, the eigenvalue inequality $\lambda_{\max}(\bar{\boldsymbol{I}}_C)\,\mathbf{x}^\top\mathbf{x} \geq \mathbf{x}^\top\,\bar{\boldsymbol{I}}_C\,\mathbf{x}$ implies

$$\lambda_{\max}(\bar{\boldsymbol{I}}_C)\mathbf{1}_3 \succeq \bar{\boldsymbol{I}}_C \tag{12}$$

Thus, through the use of (12), (11) is equivalent to

$$\tfrac{1}{2}\mathrm{Tr}(\bar{\boldsymbol{I}}_C)\,\mathbf{1}_3 - \bar{\boldsymbol{I}}_C \succeq 0 \tag{13}$$

Although (13) is mathematically equivalent to the triangle inequalities on $\bar{\boldsymbol{I}}_C$, its intuitive meaning is hardly clear in this form. The next section builds towards this intuition.

B. The Density-Weighted Covariance of a Rigid Body

It will be shown that the mathematical condition (13) can be interpreted as requiring a positive semidefinite covariance of the rigid-body mass distribution. Towards this insight, $\bar{\boldsymbol{I}}_C$ can be expanded algebraically to verify

$$\begin{aligned}\bar{\boldsymbol{I}}_C &= \textstyle\int_{\mathbb{R}^3} \mathbf{S}(\mathbf{x}_c)\mathbf{S}(\mathbf{x}_c)^\top \rho(\mathbf{x})\,\mathrm{d}\mathbf{x} \\ &= \textstyle\int_{\mathbb{R}^3} \left(\mathrm{Tr}(\mathbf{x}_c\mathbf{x}_c^\top)\mathbf{1}_3 - \mathbf{x}_c\mathbf{x}_c^\top\right)\rho(\mathbf{x})\,\mathrm{d}\mathbf{x}\end{aligned} \tag{14}$$

where $\mathbf{x}_c = \mathbf{x} - \mathbf{c}$. To simplify this expression, the *density-weighted covariance* of a rigid body is introduced as

$$\boldsymbol{\Sigma}_C = \textstyle\int_{\mathbb{R}^3} \mathbf{x}_c\,\mathbf{x}_c^\top\,\rho(\mathbf{x})\,\mathrm{d}\mathbf{x} \tag{15}$$

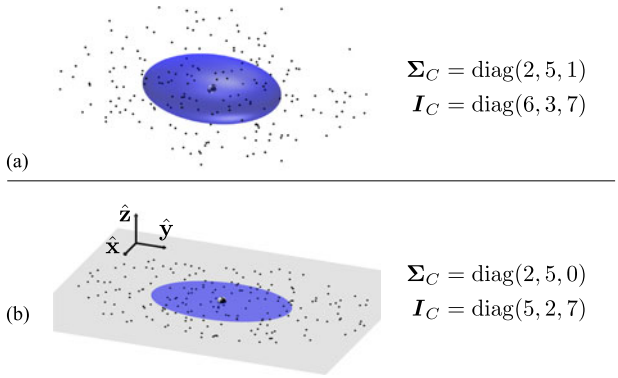

Fig. 2. Graphical representation of $\boldsymbol{\Sigma}_C$. Point-mass distribution examples with (a) $\boldsymbol{\Sigma}_C \succ 0$ for a distribution in 3D (all triangle inequalities hold strictly) (b) $\boldsymbol{\Sigma}_C \succeq 0$ for a distribution on an infinitely thin plate. Since distribution (b) is degenerate, $\boldsymbol{\Sigma}_C$ has one zero eigenvalue, and thus one triangle inequality is tight. The blue ellipsoid shown is the covariance ellipsoid $\mathcal{E}_{\boldsymbol{\pi}}$, and captures the shape of the distribution to second order.

Note that $\mathbf{c}$ is the mean position of the rigid body, in a density-weighted sense. Thus, when $m = 1$, the definition (15) matches that of covariance in probability and statistics.

The covariance $\boldsymbol{\Sigma}_C$ and rotational inertia $\bar{\boldsymbol{I}}_C$ are related through a rich set of properties. Algebraically, from (14),

$$\bar{\boldsymbol{I}}_C = \mathrm{Tr}(\boldsymbol{\Sigma}_C)\mathbf{1}_3 - \boldsymbol{\Sigma}_C \tag{16}$$

Taking the trace of both sides provides that $\mathrm{Tr}(\bar{\boldsymbol{I}}_C) = 2\,\mathrm{Tr}(\boldsymbol{\Sigma}_C)$. From (16), this property can be used to show

$$\boldsymbol{\Sigma}_C = \tfrac{1}{2}\mathrm{Tr}(\bar{\boldsymbol{I}}_C)\mathbf{1}_3 - \bar{\boldsymbol{I}}_C \tag{17}$$

which matches the form of the matrix inequality (13).

Moreover, from (16), it can be seen that $\boldsymbol{\Sigma}_C$ and $\bar{\boldsymbol{I}}_C$ share a set of eigenvectors. That is, the principal axes of $\bar{\boldsymbol{I}}_C$ are also the eigenvectors of $\boldsymbol{\Sigma}_C$. It can further be verified that if μ_1, μ_2, μ_3 are the eigenvalues of $\boldsymbol{\Sigma}_C$, then

$$J_1 = \mu_2 + \mu_3,\ J_2 = \mu_1 + \mu_3,\ J_3 = \mu_1 + \mu_2 \tag{18}$$

are the eigenvalues of $\bar{\boldsymbol{I}}_C$. Intuitively, μ_1/m gives the average squared distance to the CoM *along* the direction of the first principal axis. In comparison, J_1/m gives the average squared distance to the CoM *orthogonal to* the first principal axis. The eigenvalue relationships (18) show that there is a double counting of sorts when it comes to tallying the rotational moments of inertia. It is this double counting that is the source of the triangle inequalities.

To help visualize $\boldsymbol{\Sigma}_C$, when $\boldsymbol{\Sigma}_C \succ 0$, we define

$$\mathcal{E}_{\boldsymbol{\pi}} = \{\mathbf{x} \in \mathbb{R}^3 \,:\, (\mathbf{x} - \mathbf{c})^\top \left(\boldsymbol{\Sigma}_C/m\right)^{-1} (\mathbf{x} - \mathbf{c}) \leq 1\}$$

More generally, when $\boldsymbol{\Sigma}_C \succeq 0$ we let

$$\mathcal{E}_{\boldsymbol{\pi}} = \{\mathbf{x} \in \mathbb{R}^3 : \exists \mathbf{y},\ (\boldsymbol{\Sigma}_C/m)\mathbf{y} = (\mathbf{x} - \mathbf{c}),\ (\mathbf{x} - \mathbf{c})^\top\mathbf{y} \leq 1\}$$

The set $\mathcal{E}_{\boldsymbol{\pi}}$ is named the *covariance ellipsoid*. Mass normalization $\boldsymbol{\Sigma}_C/m$ in this definition allows $\mathcal{E}_{\boldsymbol{\pi}}$ to capture the shape of the distribution to second order while being invariant to uniform scaling in mass. The ellipsoid has semi-axes whose directions match the principal axes of $\bar{\boldsymbol{I}}_C$. However, the lengths of the semi-axes are $\sqrt{\mu_i/m}$, the root-mean-square distance to the CoM along each principal axis.

The covariance ellipsoid $\mathcal{E}_{\boldsymbol{\pi}}$ is shown in Fig. 2 for two example point-mass distributions. For simplicity of presentation, both

distributions have principal axes that are axially aligned. When $\boldsymbol{\Sigma}_C$ has a zero eigenvalue, as in Fig. 2(b), the mass distribution is degenerate. For this infinitely thin plate, the mean-squared distance to the CoM along the $\hat{\mathbf{z}}$ direction is zero. Thus, $\boldsymbol{\Sigma}_C$ has a zero eigenvalue corresponding to the $\hat{\mathbf{z}}$ principal axis. The corresponding eigenvalue in $\bar{\boldsymbol{I}}_C$ is non-zero, and measures the 2D rotational inertia of the plate about $\hat{\mathbf{z}}$. Due to the degeneracy, however, one of the triangle inequalities holds with equality. More precisely, the eigenvalue relationships (18) verify the following.

Proposition (Covariance Interpretation of Triangle Ineqs.): Suppose $\bar{\boldsymbol{I}}$, $\boldsymbol{\Sigma} \in \mathbb{S}^3$, $\boldsymbol{\Sigma} = \frac{1}{2}\mathrm{Tr}(\bar{\boldsymbol{I}})\mathbf{1}_3 - \bar{\boldsymbol{I}}$. Then $\boldsymbol{\Sigma} \succeq 0$ if and only if $\bar{\boldsymbol{I}} \succeq 0$ and $\bar{\boldsymbol{I}}$ satisfies the triangle inequalities. An analogous statement holds with all inequalities strict.

Corollary 1 (Parameterization of $\mathcal{P}^*$ with an LMI on $\boldsymbol{\Sigma}_C$): $\boldsymbol{\pi} \in \mathcal{P}^*$ if and only if $m(\boldsymbol{\pi}) > 0$ and $\boldsymbol{\Sigma}_C(\boldsymbol{\pi}) \succeq 0$.

Stating Corollary 1 plainly, physical consistency is equivalent to the mass being positive and the density-weighted covariance being positive semidefinite. Note that since any physical rigid body is non-degenerate, physical consistency can alternately be considered requiring the density-weighted covariance to be positive definite. We close this subsection with a few remarks for context.

Remark 2: A result similar to Proposition 1 can be found within [31], however, the connection to the density-weighted covariance provided here is new.

Remark 3: Corollary 1 could have applicability to inertia identification and adaptive methods for attitude control of aerial vehicles (e.g., [32], [33]). The triangle inequalities on $\bar{\boldsymbol{I}}_C$ are only treated in a small subset of the literature on this topic (e.g., [34]). Corollary 1 could be used to address the triangle inequalities in this domain.

Remark 4: Corollary 1 can also be understood within the context of probability and statistics. Suppose a density function $\rho(\cdot)$ and mass $m > 0$ with $\int \rho = m$. We can identify the density with a random variable $\mathbf{X} \in \mathbb{R}^3$ through probability density $p(\cdot) = \rho(\cdot)/m$. This association is well posed, since $\rho(\cdot)$ non-negative implies $p(\cdot)$ non-negative, and $\int p = 1$. Let $E[\cdot]$ the expectation operation and $\boldsymbol{\Sigma}(\mathbf{X}) = \mathbf{E}[(\mathbf{X} - \mathbf{E}[\mathbf{X}])(\mathbf{X} - \mathbf{E}[\mathbf{X}])^\top]$. Up to scaling by mass, Corollary 1 is equivalent to the following. Suppose $\mathbf{E} \in \mathbb{S}^3$, then there exists a random variable $\mathbf{X} \in \mathbb{R}^3$ such that $\mathbf{E} = \boldsymbol{\Sigma}(\mathbf{X})$ iff $\mathbf{E} \succeq 0$. Noting that $\boldsymbol{\Sigma}(\mathbf{X})$ is the covariance of $\mathbf{X}$, our conditions on density realizability for rigid bodies may be unsurprising in hindsight.

C. An LMI Representation of Physical Consistency

While (13) and its covariance interpretation provide a matrix inequality for the physical consistency of $\bar{\boldsymbol{I}}_C$, this condition is not linear in the inertial parameters $\boldsymbol{\pi}$. Towards an LMI over $\boldsymbol{\pi}$, a matrix of second moments is defined as

$$\boldsymbol{\Sigma} = \int_{\mathbb{R}^3} \mathbf{x}\mathbf{x}^\top \rho(\mathbf{x})\, \mathrm{d}\mathbf{x} = \int_{\mathbb{R}^3} \begin{bmatrix} x^2 & xy & xz \\ xy & y^2 & yz \\ xz & yz & z^2 \end{bmatrix} \rho(\mathbf{x})\, \mathrm{d}\mathbf{x} \tag{19}$$

Through expansion of (15) and using (5) and (6), an analog to the parallel axis theorem can be verified as:

$$\boldsymbol{\Sigma} = \boldsymbol{\Sigma}_C + m\mathbf{c}\mathbf{c}^\top \tag{20}$$

As a key feature, using the relationship $\boldsymbol{\Sigma} = \frac{1}{2}\mathrm{Tr}(\bar{\boldsymbol{I}})\mathbf{1}_3 - \bar{\boldsymbol{I}}$ from (17), $\boldsymbol{\Sigma}$ is verified linear in the inertial parameters $\boldsymbol{\pi}$.

Definition 7 (Pseudo-Inertia Matrix): The pseudo-inertia matrix $\boldsymbol{J} \in \mathbb{R}^{4\times4}$ of a rigid body is defined by

$$\boldsymbol{J} = \begin{bmatrix} \boldsymbol{\Sigma} & \mathbf{h} \\ \mathbf{h} & m \end{bmatrix}$$

Suppose some density $\rho(\cdot)$ with pseudo inertia $\boldsymbol{J}$. The entries of $\boldsymbol{J}$ are then given by definitions in (5), (6), and (19). These entries of $\boldsymbol{J}$ include all moments of $\rho(\cdot)$, in the sense of Definition 2, up to second order. Additionally, given inertial parameters $\boldsymbol{\pi} \in \mathbb{R}^{10}$, $\boldsymbol{J}(\boldsymbol{\pi})$ is verified linear in $\boldsymbol{\pi}$.

Theorem 3 (LMI Representation of $\mathcal{P}^*$): The set of physically-consistent parameters $\mathcal{P}^*$ for a single rigid body is strictly LMI representable. Its LMI representation is

$$\mathcal{P}^* = \left\{ \boldsymbol{\pi} \in \mathbb{R}^{10} \,:\, \boldsymbol{J}(\boldsymbol{\pi}) \succ 0 \right\}$$

Proof: By the Schur complement lemma [27, Section A.5.5], $\boldsymbol{J}(\boldsymbol{\pi}) \succ 0$ if and only if $m(\boldsymbol{\pi}) > 0$ and $\boldsymbol{\Sigma} - \frac{1}{m}\mathbf{h}\mathbf{h}^\top \succ 0$. By application of the parallel axis theorem for second moment matrices (20), and using $\mathbf{h} = m\mathbf{c}$, this is equivalent to $\boldsymbol{\Sigma}_C \succ 0$. From Proposition 1, this is equivalent to $\bar{\boldsymbol{I}}_C \succ 0$ and $\bar{\boldsymbol{I}}_C$ satisfies the triangle inequalities. Finally, from the main result of [14], this is equivalent to $\boldsymbol{\pi} \in \mathcal{P}^*$. ■

Remark 5: Again, taking a statistical perspective on the mass distribution, the results of Theorem 3 can be seen to follow from a condition on the first and second moments in probability and statistics [35, Theorem 16.1.2]. Suppose $\boldsymbol{\mu} \in \mathbb{R}^3$ and $\mathbf{E} \in \mathbb{S}^3$, then there exists a random variable $\mathbf{X} \in \mathbb{R}^3$ such that $\boldsymbol{\mu} = E[\mathbf{X}]$ and $\mathbf{E} = E[\mathbf{X}\mathbf{X}^\top]$ if and only if

$$\begin{bmatrix} \mathbf{E} & \boldsymbol{\mu} \\ \boldsymbol{\mu}^\top & 1 \end{bmatrix} \succeq 0$$

In comparison, the constraint $\boldsymbol{J}(\boldsymbol{\pi}) \succ 0$ in Theorem 3 is scaled by mass and enforces non-degeneracy of the distribution.

The moment matrix $\boldsymbol{J}(\boldsymbol{\pi})$ was found commonly in early robot dynamics literature (e.g., [36], [37]). It has been employed in 4×4 matrix forms of the dynamics for a rigid body [38], [39]. Using these 4×4 equations, a parameter identification approach for a single rigid body was proposed in [39]. The pseudo inertia was used to provide a left-invariant Riemannian metric over $\mathsf{SE}(3)$ [31] and appears in robotics books (e.g., [40]). Despite its importance here, the pseudo inertia is notably lacking from current mainstream literature on robot dynamics.

It is interesting to note how the pseudo inertia $\boldsymbol{J}(\boldsymbol{\pi})$ compares to the standard spatial inertia $\boldsymbol{I}(\boldsymbol{\pi})$ in terms of the kinetic energy metric each provides. Suppose

$$\mathbf{v} = \begin{bmatrix} \boldsymbol{\omega} \\ \boldsymbol{v} \end{bmatrix} \in \mathbb{R}^6 \,, \text{and } \mathbf{V} = \begin{bmatrix} \mathbf{S}(\boldsymbol{\omega}) & \boldsymbol{v} \\ \mathbf{0} & 0 \end{bmatrix} \in \mathsf{se}(3)$$

It can be verified that the kinetic energy satisfies [40]

$$\tfrac{1}{2}\mathbf{v}^\top \boldsymbol{I}(\boldsymbol{\pi})\mathbf{v} = \tfrac{1}{2}\mathrm{Tr}\big(\mathbf{V}\, \boldsymbol{J}(\boldsymbol{\pi})\mathbf{V}^\top\big)$$

Thus, while physical semi-consistency ensures that the associated kinetic energy metric is positive definite, additional constraints from the triangle inequalities enforce added structure on the metric. As has been shown for the first time here, the triangle inequalities are precisely what represent the difference between $\boldsymbol{I}(\boldsymbol{\pi}) \succ 0$ and $\boldsymbol{J}(\boldsymbol{\pi}) \succ 0$. The pseudo inertia is also of a lower dimension (4×4) than the spatial inertia (6×6). This

provides computational benefits to enforcing LMIs on $\boldsymbol{J}(\boldsymbol{\pi})$ in comparison to $\boldsymbol{I}(\boldsymbol{\pi})$.

V. Contribution: LMI Constraints for Inertial Parameter Realizability on Ellipsoids

It has been shown that physical consistency of the inertial parameters can be enforced with an LMI over all moments up to second order. The resultant LMIs have been explained through connections to the existence of probability measures. Even beyond mechanics and probability, however, the realizability of moment sequences represents a more general problem in mathematics. Namely, it represents the classical problem of moments (see e.g., [26], [41]). With this insight, results are translated here to provide new conditions on density realizability with bounding-volume constraints.

Recent work has shown the benefits of including prior knowledge on the shape of each rigid body within parameter identification. Work by Jovic *et al.* [12] for instance, enforced the CoM to reside within a bounding box estimated from CAD. New constraints are provided here that address second moments.

To begin, suppose a rigid body is known to reside within an ellipsoid $\mathcal{S} \subset \mathbb{R}^3$ described by:

$$\mathcal{S} = \{\mathbf{x} \in \mathbb{R}^3 \,|\, (\mathbf{x} - \mathbf{x}_s)^\top \mathbf{Q}_s^{-1} (\mathbf{x} - \mathbf{x}_s) \leq 1\} \tag{21}$$

Before considering constraints on the second moments, it is noted that the CoM constraint, $\mathbf{c}(\boldsymbol{\pi}) \in \mathcal{S}$, can be formulated as an LMI over $\boldsymbol{\pi}$. When $m(\boldsymbol{\pi}) > 0$, $\mathbf{c}(\boldsymbol{\pi}) \in \mathcal{S}$ iff

$$\boldsymbol{C}(\boldsymbol{\pi}) = \begin{bmatrix} m(\boldsymbol{\pi}) & \mathbf{h}(\boldsymbol{\pi})^\top - m(\boldsymbol{\pi})\mathbf{x}_s^\top \\ \mathbf{h}(\boldsymbol{\pi}) - m(\boldsymbol{\pi})\mathbf{x}_s & m(\boldsymbol{\pi})\mathbf{Q}_s \end{bmatrix} \succeq 0 \tag{22}$$

Again, equivalence is due to the Schur complement lemma.

Yet, as the CoM approaches the edge of $\mathcal{S}$, large second moments would imply the existence of mass outside the ellipsoid. In fact, as the CoM of a rigid body approaches the edge of a bounding ellipsoid, the rigid body necessarily degenerates to a point mass. Thus, constraints that $\mathbf{c}(\boldsymbol{\pi}) \in \mathcal{S}$ alone are not sufficient for $\boldsymbol{\pi}$ to be $\mathcal{S}$-density realizable. Drawing on the classical problem of moments, Theorem 4.7(b) from [26] can be translated as follows.

Theorem 4 (Density Realizability on an Ellipsoid): Suppose a bounding ellipsoid $\mathcal{S} \subset \mathbb{R}^3$. Let $\mathbf{Q} \in \mathbb{R}^{4\times4}$ such that

$$\mathcal{S} = \left\{ \mathbf{x} \in \mathbb{R}^3 \,:\, \begin{bmatrix} \mathbf{x} \\ 1 \end{bmatrix}^\top \mathbf{Q} \begin{bmatrix} \mathbf{x} \\ 1 \end{bmatrix} \geq 0 \right\}$$

Then, $\boldsymbol{\pi}$ is $\mathcal{S}$-density realizable if and only if

$$\boldsymbol{J}(\boldsymbol{\pi}) \succ 0 \,\text{and}\, \mathrm{Tr}\left(\boldsymbol{J}(\boldsymbol{\pi})\,\mathbf{Q}\right) \geq 0\,. \tag{23}$$

Further, any $\boldsymbol{\pi}$ is $\mathcal{S}$-density realizable iff it can be represented by four point masses m_k at positions $\mathbf{x}_k \in \mathcal{S}$.

Proof: See [26, Theorem 4.7(b)]. ■

Note that by taking into account second moments, the condition $\mathrm{Tr}(\boldsymbol{J}(\boldsymbol{\pi})\,\mathbf{Q}) \geq 0$ in (23) is a 1D linear inequality constraint. The looser condition (22) is a 4×4 LMI. Thus, the new conditions are both tighter, and computationally more efficient to enforce. Fig. 3 shows a number of cases, illustrating both the role of the CoM location and the shape of the covariance ellipsoid $\mathcal{E}_{\boldsymbol{\pi}}$ on $\mathcal{S}$-density realizability. The following corollary is provided to accommodate more complex bounding shapes.

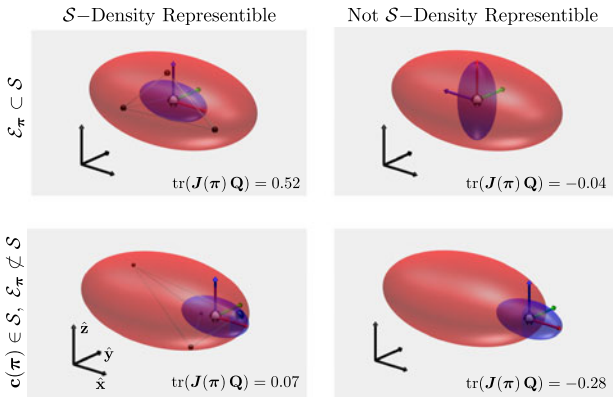

Fig. 3. Cases illustrating the role of the center and shape of the covariance ellipsoid $\mathcal{E}_{\boldsymbol{\pi}}$ on $\mathcal{S}$-density realizability of $\boldsymbol{\pi}$. In each case, the ellipsoid $\mathcal{S}$ has semi-axes of length $\sqrt{5}, \sqrt{2}, 1$ in the $\hat{\mathbf{x}}, \hat{\mathbf{y}}, \hat{\mathbf{z}}$ directions. $\mathcal{E}_{\boldsymbol{\pi}}$ has semi-axes $\sqrt{0.9}, \sqrt{0.2}, \sqrt{0.2}$ with principle axes colored accordingly in the figure. When a mass distribution on $\mathcal{S}$ exists, a distribution by four point masses is shown, as guaranteed to exist through Theorem 4.

Corollary 2 (Density Realizability on the Union of Ellipsoids). Suppose a rigid body is known to reside within the union of n_ℓ ellipsoids $\mathcal{S} = \cup_{j=1}^{n_\ell} \mathcal{S}_j$. Then, its inertial parameters $\boldsymbol{\pi}$ are $\mathcal{S}$-density realizable if and only if there exist parameters $\{\boldsymbol{\pi}_j\}_{j=1}^{n_\ell}$ such that $\boldsymbol{\pi} = \sum_j \boldsymbol{\pi}_j$ and each $\boldsymbol{\pi}_j$ is $\mathcal{S}_j$-density realizable as verified by Theorem 4.

Remark 6: LMIs for the nested sets $\mathcal{P}^*_{\mathcal{S}} \subset \mathcal{P}^*_{\mathbb{R}^3} \subset \mathcal{P}$ have applicability for other problems. Tightened convex constraints can only increase the rate of convergence for online parameter estimation [24], or more generally provide faster decrease of Lyapunov-like functions in adaptive control [25]. For a system of bodies, the relative volume of the set $\mathcal{P}^*_{\mathcal{S}_1} \times \cdots \times \mathcal{P}^*_{\mathcal{S}_{n_b}}$ versus $\mathcal{P}^*_{\mathbb{R}^3} \times \cdots \times \mathcal{P}^*_{\mathbb{R}^3}$ decreases exponentially with n_b due to its product structure. Thus, it is expected that these benefits will increase for higher-DoF robots.

VI. Experimental Validation

The proposed constraints were applied to identify a leg of the MIT Cheetah 3 robot. The robot, shown in Fig. 1, has four 3-DoF legs where each DoF is driven by a proprioceptive actuator [9]. Each actuator includes a high-inertia rotor coupled to the joint by a $10.6:1$ gearbox. To address actuator effects, the leg was treated as a system of $n_b = 6$ bodies (3 links and 3 rotors). Joint rates at the gearbox output were used for $\boldsymbol{\nu} \in \mathbb{R}^3$. To account for transmission losses, (2) was modified via diagonal matrices of viscous and Coulomb friction coefficients $\mathbf{B} \in \mathbb{R}^{3\times3}$ and $\mathbf{B}_c \in \mathbb{R}^{3\times3}$

$$\boldsymbol{\tau} - \mathbf{B}\,\boldsymbol{\nu} - \mathbf{B}_c\,\mathrm{sign}(\boldsymbol{\nu}) = \mathbf{Y}(\mathbf{q}, \boldsymbol{\nu}, \dot{\boldsymbol{\nu}})\,\boldsymbol{\pi} \tag{24}$$

Using Theorem 4, physically realistic inertial parameters can be identified alongside transmission effects.

$$\begin{aligned} \min_{\boldsymbol{\pi}, \mathbf{B}_c, \mathbf{B}} \; & \frac{1}{n_s} \sum_m \|\mathbf{Y}^{(m)}\,\boldsymbol{\pi} + \mathbf{B}\,\boldsymbol{\nu}^{(m)} + \mathbf{B}_c\,\mathrm{sign}(\boldsymbol{\nu}^{(m)}) - \boldsymbol{\tau}^{(m)}\|^2 \\ & + w_\pi \|\boldsymbol{\pi} - \hat{\boldsymbol{\pi}}\|^2 \\ \text{s.t.} \; & \boldsymbol{C}_i(\boldsymbol{\pi}_i) \succeq 0 \\ & \boldsymbol{J}(\boldsymbol{\pi}_i) \succ 0 \\ & \mathrm{Tr}(\boldsymbol{J}(\boldsymbol{\pi}_i)\,\mathbf{Q}_i)\; 0 \quad \forall i \in \{1, \ldots, n_b\} \end{aligned} \tag{25}$$

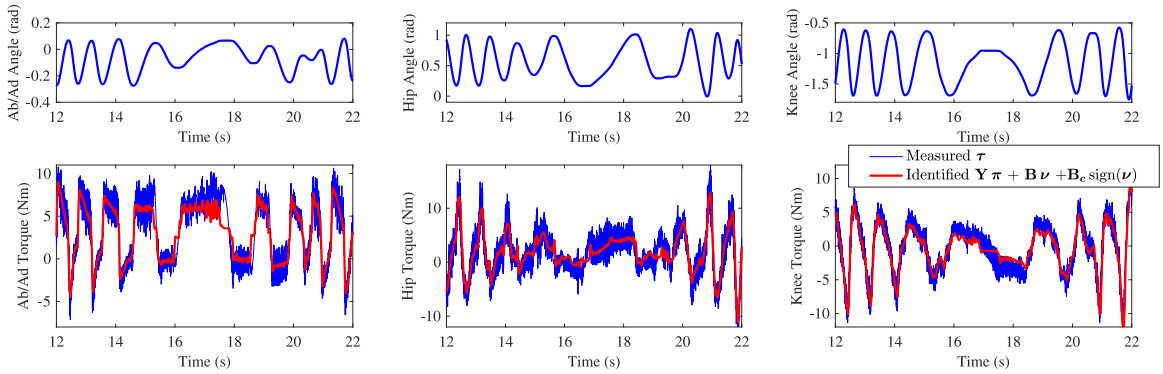

Fig. 4. Regression errors after identification of a leg for the MIT Cheetah 3. The data shown is distinct from that used in training. Motor torques are predicted with an overall RMS error of 1.46 Nm. For comparison, the Coulomb friction was identified as $\mathbf{B}_c = \text{diag}(3.12, 1.25, 0.95)$ Nm.

A small regularizing term $w_\pi \|\boldsymbol{\pi} - \hat{\boldsymbol{\pi}}\|^2$ was added where $\hat{\boldsymbol{\pi}} \in \mathbb{R}^{10n_b}$ is a set of estimated inertial parameters from CAD or other sources. Such regularization is common practice [13]. Bounding-ellipsoid parameters for the CoM and body, in $\boldsymbol{C}_i$ and $\mathbf{Q}_i$ respectively, were set using geometry from CAD.

Data was gathered from a leg swinging experiment shown in the supplementary video. The leg was placed in a Cartesian impedance control mode, and the foot endpoint was commanded to move on a virtual ellipsoidal shell. The target point on the shell was set through spherical angles (ϕ, θ), using rates $\dot{\phi} = A_\phi \sin(\omega_\phi t)$ and $\dot{\theta} = A_\theta \sin(\omega_\theta t)$ with $A_\phi = 12$ rad/s, $A_\theta = 3.4$ rad/s, $\omega_\phi = 1.63$ rad/s, and $\omega_\theta = 0.265$ rad/s. Data was sampled at 1 kHz. Joint actuator torques $\boldsymbol{\tau}_j$ were estimated from the torques commanded to motor drivers [9]. At each data point, a modified version of the Recursive-Newton-Euler Algorithm [29] was used to compute each column of $\mathbf{Y}$. Following this computation, the problem (25) was solved with 10,000 samples using MOSEK [42] in MATLAB. The problem took 1.67 s to solve to global optimality on a 2011 Intel Core i5 MacBook Pro. Regularization of $w_\pi = 10^{-6}$ was used. It was verified that all physical-consistency constraints were satisfied. Numeric values for the identified parameters are provided in the supplementary material.

After identification, the RMS errors from (24) with the *next* 10,000 samples in the dataset were 1.48, 1.69, and 1.16 Nm on the ab/ad, hip, and knee respectively. For comparison, Coulomb friction was found as $\mathbf{B}_c = \text{diag}(3.12, 1.25, 0.95)$ Nm. Fig. 4 shows validation results. The measured $\boldsymbol{\tau}$, used as input to the algorithm, shows high-frequency noise. This noise is from finite-differenced encoder signals used in online feedback. In contrast, the estimated data used non-causally filtered signals to compute $\mathbf{Y}$ offline. This results in a comparatively smoother identified estimate.The estimation is notably poor on the ab/ad joint at 17.5 s. However, this occurs at a time when the joint is not moving, and the sign of the Coulomb friction torque cannot be reliably predicted.

Fig. 5 shows an accounting of friction and inertial effects on the identified model. Effects that dominate the required torques are shown to be dependent on both the motion as well as the joint. This demonstrates the need to identify all model components treated here. It is important to note that these effects will be robot and transmission specific.

Fig. 6 shows the validation error with different training sample sizes n_s and different constraints. As in Remark 6, tighter constraints empirically result in an accurate model more rapidly

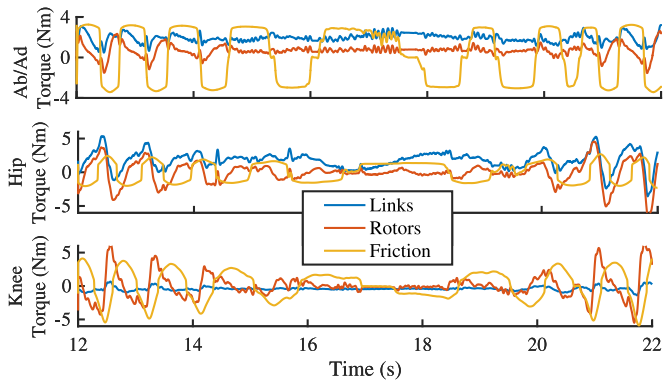

Fig. 5. Identified contributions of the effects from link inertias, rotor inertias, and friction. Data is from the same experiment as Fig. 4.

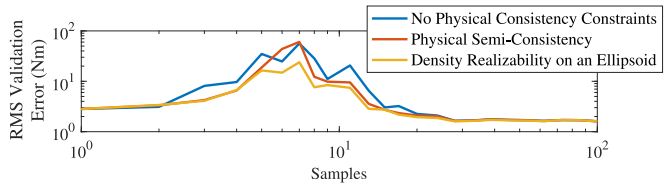

Fig. 6. Validation error (after identification) versus training sample size.

as samples are added. Lower validation error for tighter constraints further demonstrates reduced overfitting. These benefits are in addition to the fact that tighter constraints result in physically realistic model parameters.

Remark 7: Although these results have only addressed a 3-DoF leg, physical-consistency constraints are equally applicable to more complex rigid-body systems. Previous work demonstrated the scalability of least-squares identification to high-DoF platforms [11], [12]. The 4×4 LMIs proposed would present minor added overhead to the solution of these problems. As in Remark 6, benefits from our tightened constraints are expected to increase with the number of bodies.

VII. CONCLUSION

This letter has introduced LMIs to rigorously characterize physical consistency of rigid-body inertial parameters. Rather than focusing on the moments of inertia, physical plausibil-

ity is directly assessed using the types of moments encountered in probability and statistics. With this observation, LMIs involving a pseudo-inertia matrix and its density-weighted covariance have been shown to tightly characterize physical consistency. LMI constraints for density realizability on an ellipsoid were also proposed through connections to the classical problem of moments in mathematics.

In closing, recall that while intuition was borrowed from probability and statistics, there is nothing stochastic about our results. Given a bounding ellipsoid for a rigid body, the new constraints characterize a cone where its inertial parameters must reside with certainty. Beyond least-squares considerations, a quantified treatment of stochasticity can play an important role in inferring models from uncertain measurements, with a rich literature on the topic (e.g., [17]–[21]). The incorporation of rigorous physical-consistency considerations into this inference represents an interesting next step for inertial parameter identification.

REFERENCES

[1] Y. Abe, M. da Silva, and J. Popović, "Multiobjective control with frictional contacts," in *Proc. 2007 ACM SIGGRAPH/Eurograph. Symp. Comput. Animation*, Aire-la-Ville, Switzerland, 2007, pp. 249–258.

[2] J. Park, J. Haan, and F. Park, "Convex optimization algorithms for active balancing of humanoid robots," *IEEE Trans. Robot.*, vol. 23, no. 4, pp. 817–822, Aug. 2007.

[3] L. Sentis, J. Park, and O. Khatib, "Compliant control of multicontact and center-of-mass behaviors in humanoid robots," *IEEE Trans. Robot.*, vol. 26, no. 3, pp. 483–501, Jun. 2010.

[4] P. M. Wensing and D. E. Orin, "Generation of dynamic humanoid behaviors through task-space control with conic optimization," in *Proc. IEEE Int. Conf. Rob. Autom.*, May 2013, pp. 3103–3109.

[5] M. Hutter, H. Sommer, C. Gehring, M. Hoepflinger, M. Bloesch, and R. Siegwart, "Quadrupedal locomotion using hierarchical operational space control," *Int. J. Robot. Res.*, vol. 33, no. 8, pp. 1047–1062, 2014.

[6] J. Koenemann *et al.*, "Whole-body model-predictive control applied to the HRP-2 humanoid," in *Proc. IEEE/RSJ Int. Conf. Intell. Robots Syst.*, Sep. 2015, pp. 3346–3351.

[7] S. Kuindersma *et al.*, "Optimization-based locomotion planning, estimation, and control design for the atlas humanoid robot," *Autonomous Robots*, vol. 40, pp. 429–455, 2016.

[8] A. Herzog, N. Rotella, S. Mason, F. Grimminger, S. Schaal, and L. Righetti, "Momentum control with hierarchical inverse dynamics on a torque-controlled humanoid," *Autonomous Robots*, vol. 40, no. 3, pp. 473–491, 2016.

[9] P. M. Wensing, A. Wang, S. Seok, D. Otten, J. Lang, and S. Kim, "Proprioceptive actuator design in the MIT Cheetah: Impact mitigation and high-bandwidth physical interaction for dynamic legged robots," *IEEE Trans. Robot.*, vol. 33, no. 3, pp. 509–522, Jun. 2017.

[10] D. Pucci, F. Romano, and F. Nori, "Collocated adaptive control of underactuated mechanical systems," *IEEE Trans. Robot.*, vol. 31, no. 6, pp. 1527–1536, Dec. 2015.

[11] K. Ayusawa, G. Venture, and Y. Nakamura, "Identifiability and identification of inertial parameters using the underactuated base-link dynamics for legged multibody systems," *Int. J. Robot. Res.*, vol. 33, no. 3, pp. 446–468, 2014.

[12] J. Jovic, A. Escande, K. Ayusawa, E. Yoshida, A. Kheddar, and G. Venture, "Humanoid and human inertia parameter identification using hierarchical optimization," *IEEE Trans. Robot.*, vol. 32, no. 3, pp. 726–735, Jun. 2016.

[13] C. D. Sousa and R. Cortesão, "Physical feasibility of robot base inertial parameter identification: A linear matrix inequality approach," *Int. J. Robot. Res.*, vol. 33, no. 6, pp. 931–944, 2014.

[14] S. Traversaro, S. Brossette, A. Escande, and F. Nori, "Identification of fully physical consistent inertial parameters using optimization on manifolds," in *Proc. IEEE/RSJ Int. Conf. Intell. Rob. Sys.*, Oct. 2016, pp. 5446–5451.

[15] C. G. Atkeson, C. H. An, and J. M. Hollerbach, "Estimation of inertial parameters of manipulator loads and links," *Int. J. Robot. Res.*, vol. 5, no. 3, pp. 101–119, 1986.

[16] M. Gautier and W. Khalil, "Exciting trajectories for the identification of base inertial parameters of robots," in *Proc. 30th IEEE Conf. Decision Control*, Dec. 1991, vol. 1, pp. 494–499.

[17] J. Swevers, C. Ganseman, D. B. Tukel, J. de Schutter, and H. V. Brussel, "Optimal robot excitation and identification," *IEEE Trans. Robot. Autom.*, vol. 13, no. 5, pp. 730–740, Oct. 1997.

[18] J. Ting, M. Mistry, J. Peters, S. Schaal, and J. Nakanishi, "A Bayesian approach to nonlinear parameter identification for rigid body dynamics," in *Proc. Robot., Science Syst.*, 2006, pp. 32:1–32:8.

[19] A. Janot, P. O. Vandanjon, and M. Gautier, "A generic instrumental variable approach for industrial robot identification," *IEEE Trans. Control Syst. Technol.*, vol. 22, no. 1, pp. 132–145, Jan. 2014.

[20] G. Calafiore and M. Indri, "Robust calibration and control of robotic manipulators," in *Proc. Amer. Control Conf.*, 2000, pp. 2003–2007.

[21] N. Ramdani and P. Poignet, "Robust dynamic experimental identification of robots with set membership uncertainty," *IEEE/ASME Trans. Mechatronics*, vol. 10, no. 2, pp. 253–256, Apr. 2005.

[22] J.-J. E. Slotine and W. Li, "On the adaptive control of robot manipulators," *Int. J. Robot. Res.*, vol. 6, no. 3, pp. 49–59, 1987.

[23] K. Ayusawa, G. Venture, and Y. Nakamura, "Real-time implementation of physically consistent identification of human body segments," in *Proc. IEEE Inf. Conf. Robot. Autom.*, May 2011, pp. 6282–6287.

[24] P. A. Ioannou and J. Sun, *Robust Adaptive Control*. Courier, Dover: Mineola, NY, 2012.

[25] J.-J. E. Slotine and J. A. Coetsee, "Adaptive sliding controller synthesis for non-linear systems," *Int. J. Control*, vol. 43, no. 6, pp. 1631–1651, 1986.

[26] L. Fialkow and J. Nie, "Positivity of Riesz functionals and solutions of quadratic and quartic moment problems," *J. Funct. Anal.*, vol. 258, no. 1, pp. 328–356, 2010.

[27] S. Boyd and L. Vandenberghe, *Convex Optimization*. Cambridge, U.K.: Cambridge Univ. Press, 2004.

[28] S. Boyd, L. E. Ghaoui, E. Feron, and V. Balakrishnan, *Linear Matrix Inequalities in System and Control Theory* (ser. Studies in Applied and Numerical Mathematics). Philadelphia, PA, USA: SIAM, 1994.

[29] R. Featherstone, *Rigid Body Dynamics Algorithms*. New York, NY, USA: Springer, 2008.

[30] W. Li and J.-J. E. Slotine, "An indirect adaptive robot controller," *Syst. Control Lett.*, vol. 12, no. 3, pp. 259–266, 1989.

[31] C. Belta and V. Kumar, "An SVD-based projection method for interpolation on SE(3)," *IEEE Trans. Robot. Autom.*, vol. 18, no. 3, pp. 334–345, Jun. 2002.

[32] N. A. Chaturvedi, D. S. Bernstein, J. Ahmed, F. Bacconi, and N. H. McClamroch, "Globally convergent adaptive tracking of angular velocity and inertia identification for a 3-dof rigid body," *IEEE Trans. Control Syst. Technol.*, vol. 14, no. 5, pp. 841–853, Sep. 2006.

[33] D. Thakur, S. Srikant, and M. R. Akella, "Adaptive attitude-tracking control of spacecraft with uncertain time-varying inertia parameters," *J. Guidance, Control, Dyn.*, vol. 38, no. 1, pp. 41–52, 2014.

[34] Z. Manchester and M. Peck, "Recursive inertia estimation with semidefinite programming," in *Proc. AIAA Guidance, Navigation, Control Conf.*, 2017, doi: https://doi.org/10.2514/6.2017-1902.

[35] D. Bertsimas and J. Sethuraman, "Moment problems and semidefinite optimization," in *Handbook Semidefinite Programming* (ser. International Series in Operations Research & Management Science), vol. 27, H. Wolkowicz, R. Saigal, and L. Vandenberghe, Eds. New York, NY, USA: Springer, 2000, pp. 469–509.

[36] A. K. Bejczy, "Robot arm dynamics and control," JPL Technical Memorandum, Pasadena, CA, 1974, Tech. Rep. 33–669.

[37] J. J. Uicker, Jr, "Dynamic force analysis of spatial linkages," *J. Appl. Mech.*, vol. 34, no. 2, pp. 418–424, Jun. 1967.

[38] G. Legnani, F. Casolo, P. Righettini, and B. Zappa, "A homogeneous matrix approach to 3D kinematics and dynamics—I. Theory," *Mech. Mach. Theory*, vol. 31, no. 5, pp. 573–587, 1996.

[39] E. Atchonouglo, C. Vallée, T. Monnet, and D. Fortuné, "Identification of the ten inertia parameters of a rigid body," *J. Appl. Math. Mech.*, vol. 72, no. 1, pp. 22–25, 2008.

[40] T. Yoshikawa, *Dynamics*. Cambridge, MA, USA: MIT Press, 2003, pp. 81–126.

[41] J. B. Lasserre, "A semidefinite programming approach to the generalized problem of moments," *Math. Program.*, vol. 112, no. 1, pp. 65–92, 2008.

[42] E. D. Andersen, C. Roos, and T. Terlaky, "On implementing a primal-dual interior-point method for conic quadratic optimization," *Math. Program.*, vol. 95, no. 1, pp. 249–277, 2003.